1 Introduction to Injection Molding

Shia-Chung Chen

1.1 Injection Molding and Molding Machines

Injection molding is an important thermoplastic processing technique for producing plastic parts and products [1, 2]. Complete operation of injection molding requires an injection molding machine with a control unit, a properly clamped mold with a cavity or cavities that define(s) the part geometry, and a mold temperature control unit. The process begins with feeding plastic pellets of about 2 to 3 mm in size into the hopper of the injection molding machine (Figure 1.1). Before feeding, the plastic pellets are dried and cleaned to ensure low moisture content. Additives may be added to the pellets to be fed into the hopper to modify the plastic's or final product's properties.

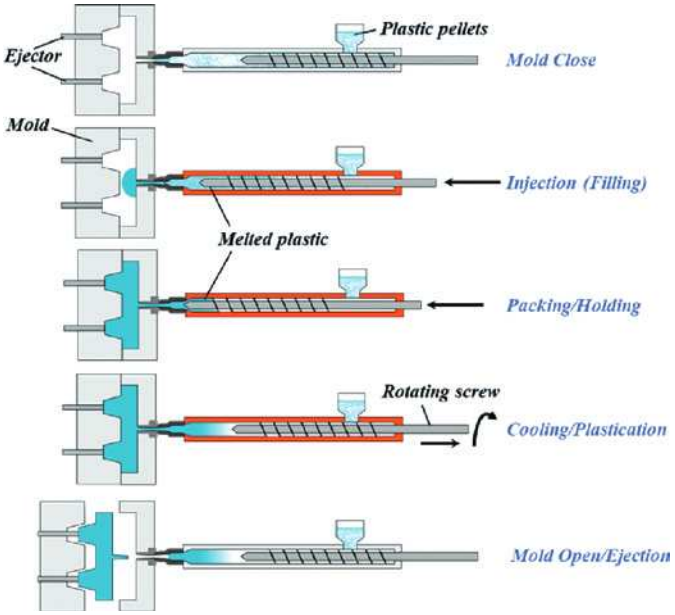

Figure 1.1 Schematic of the injection molding process [3]

The injection screw then rotates and conveys the pellets to the heated barrel of the injection molding machine. The barrel consists of three zones—the feeding zone, the compression zone (transition zone), and the metering zone—all of which may be set to different heating temperatures (Figure 1.2). As the pellets pass through the feeding and compression zones, they gradually melt until they finally become a hot melt within the metering zone. The rotation of the screw provides shear heating resulting from the mechanical crushing of the pellets between the screw flights and the barrel. The shear heating acts as the major heat source for pellet melting. Additional heat is also transferred from the barrel to the pellets via contact, which assists in melting the pellets. The rotation of the screw stops when the proper amount of melt is accumulated from the tip of the screw to the nozzle. The accumulation and conveying of melt within the barrel builds up pressure in front of the screw tip. The pressure pushes back the screw until enough melt for one shot is accumulated. This melt preparation stage is also known as the plasticating stage. In front of the screw tip, there is a shut-off valve to prevent melt entering into the mold during the plasticating stage.

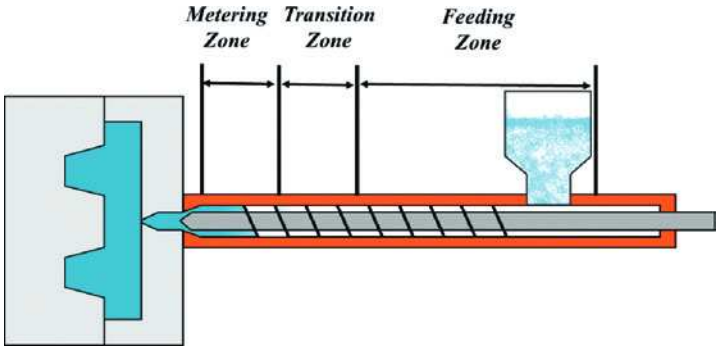

Figure 1.2 Schematic of the three main zones within the injection molding barrel [3]

Once the screw stops rotating, the hydraulic pressure or electrical motor acts to move the screw forward at the profiled speed and push the plastic melt to flow through the nozzle, the sprue, the runner system, and into the cavity. The stage in which the melt begins to flow through the sprue until the cavity is entirely filled is called the mold filling stage. Once the cavity is filled, the screw continues to push additional melt into the cavity under very low speed (pressure-activated) to compensate for the subsequent shrinkage due to melt solidification. The slow advance of the screw under the profiled pressure is called the mold packing/holding stage. The packing stage ends when the gate is completely frozen and no more melt can be pushed into the cavity. The filled melt within the cavity is cooled until the part surface is sufficiently solidified. Then the mold is opened and the part is ejected. This stage of melt solidification is known as the mold cooling stage. The plastic

melt begins to cool as soon as it touches the cold surface of the mold cavity. However, the serious cooling begins when the filling of the cavity ends. The cessation of hot melt flow also indicates that no more heat is being conducted into the cavity. Although cooling continues throughout the entire injection cycle, the cooling stage is usually recognized as the period between the end of the packing stage and the beginning of part ejection.

When the gate is frozen, the screw can begin rotating and plasticating the melt for the next injection cycle. Thus, one injection cycle (Figure 1.3) includes mold closing, mold filling, mold packing, mold cooling, and mold opening. Plastication begins during the mold cooling stage and may last until mold opening or even before the end of mold closing of the next cycle. Plastic shrinks as it cools from the melt temperature to a solid state. The relationship between pressure, temperature, and specific volume (discussed later), as well as the thermal-mechanical history of material elements, determine the volumetric shrinkage of the parts. During the injection molding process, pressure and temperature gradients exist within the melt and the solidified parts, resulting in non-uniform part shrinkage and associated warpage, which are important issues to be resolved and controlled within acceptable limits during the molding process.

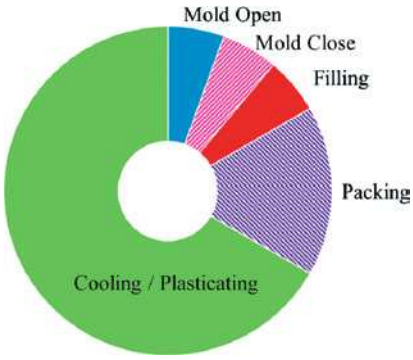

Figure 1.3
Injection molding cycle

1.1.1 Brief Overview of an Injection Molding Machine

The most popular type of injection molding machine at present is the reciprocating screw injection machine, prototypes of which first appeared in the 1940s and 1950s. The two essential components of an injection molding machine are the injection unit and the clamping unit, whose operation relies on the hydraulic or electrical servomotor system and the associated control system.

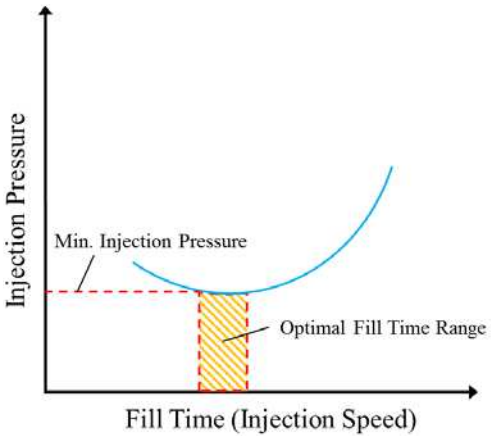

Figure 1.5
Injection pressure needed for different fill times

1.1.2.4 Mold Temperature

Coolants circulate in the cooling channels to maintain the cavity surface temperature. Cavity surface temperature is determined by coolant temperature, coolant thermal and rheological properties, coolant flow rate, and the corresponding cooling channel dimensions and layout. The mold materials, mold size, and the duration of melt within the cavity, as well as factors such as initial melt temperature, ejection temperature, and part thickness, may also influence the cavity surface temperature. During molding operation, the heat from the hot melt flow should be approximately equal to the heat removed by the coolants. Thus, the coolant flow rate in each branch of the cooling channel should have a high Reynolds number to ensure that the flow is turbulent. Cavity surface temperature is not only intimately related to the cooling time but also significantly affects the part quality. Mold temperature varies in a transient cyclic manner (Figure 1.6) and also varies from location to location within the mold. Thus, the design of cooling channels to achieve uniform cooling and to maintain a relatively constant mold temperature is crucial.

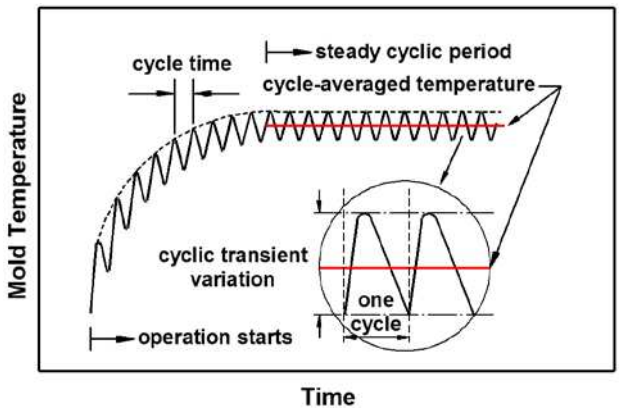

Figure 1.6
Mold temperature variation versus injection cycle [5]

An accurate and robust key process variable control system is necessary to ensure the repeatability and reliability of the product quality, and it forms the foundation layer of the overall control and monitoring system. Up to now, most of the research has been focused on the individual process variable control. Recently, some new control strategies were developed that exploit the inherent characteristics of the injection molding process. This chapter reviews the development of control strategies in injection molding applications. The rest of this chapter is constructed as follows: Section 2.2 introduces the traditional feedback control strategies with the adaptive model predictive control as an example, Section 2.3 illustrates the application of a fuzzy inference system in injection molding control, Section 2.4 shows the learning-type control, Section 2.5 introduces a recently developed two-dimensional control algorithm, and Section 2.6 gives the summary and perspectives.

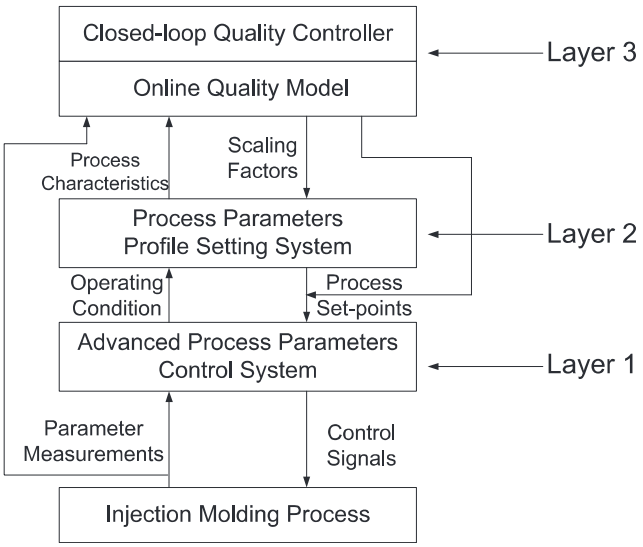

Figure 2.2 Block diagram of a multilayer control system structure

2.2 Feedback Control Algorithms: Adaptive Control

Feedback control is an important class of control algorithms in which the controller receives the signal of the measurement unit and compares it with the desired values to make the control decision. Thus the current control decisions are made based on the observations of the effects of previous decisions. The proportional-integral-derivative (PID) controller is the most widely used feedback control strategy.

It was first developed for automatic ship steering, and it is the most standard feedback control algorithm. It measures the controlled variable, calculates the error between the output and set point, and generates the controller output based on the proportional, the integral, and derivative of the errors. As a simple and general-purpose control algorithm, PID may be the most successful automatic controller in industry. For the injection molding process, PID control is commonly used in the barrel and mold temperature control. In the early practice, it was also used to control some key process variables, such as injection velocity and packing pressure. However, it also has some significant limitations. For example, it only works for linear and time-invariant processes and is not suitable for complex and nonlinear processes like injection molding. Also, the parameters of the PID controller are fixed, so it cannot be used as the core of an advanced control system. The PID control is suitable for continuous processes, since for the continuous process, normally working around a certain operating point, the process dynamics can be linearized in a small range, and PID control can be effective under such circumstances. As a typical batch process, injection molding is stage-based and often operating over a wide range of conditions, so the traditional fixed-parameter controller cannot ensure a satisfactory performance [2].

Due to the batch nature and the nonlinear and time-varying characteristics of the injection molding process, advanced feedback control strategies must be applied to ensure good control performance. Adaptive control is a proper candidate since its parameters are adapted in a certain way to conform to the nonlinear or time-varying process dynamics. There are many different types of adaptive control schemes, such as gain scheduling, model reference adaptive control, dual adaptive control, and self-tuning regulators (STR). The STR, as an important scheme of adaptive control, is used for illustration in this chapter to control some key process variables in injection molding. The basic principle of STR is briefly described in the following sections, and detailed discussions can be found in reference [4].

A self-tuning system is graphically shown in Figure 2.3 [4]. The system is composed of two loops: an ordinary feedback control loop as shown inside the dashed line, and a controller parameter adjusting loop as shown inside the dotted line. The latter, consisting of a parametric model estimator and a controller design calculator, gives an online adjustment of the parameters of the feedback controller. The process model parameters and controller design are updated during each sampling period, with a specified model structure.

There are several methods for process model parameter estimation, for example, least mean squares (LMS), projection algorithm (PA), and stochastic approximation (SA). In this chapter, a recursive least-squares (RLS) estimator is used due to its good sensitivity and superior convergence property [4]. A model predictive control (MPC) design is adopted for the controller design to demonstrate the working procedure of the STR.

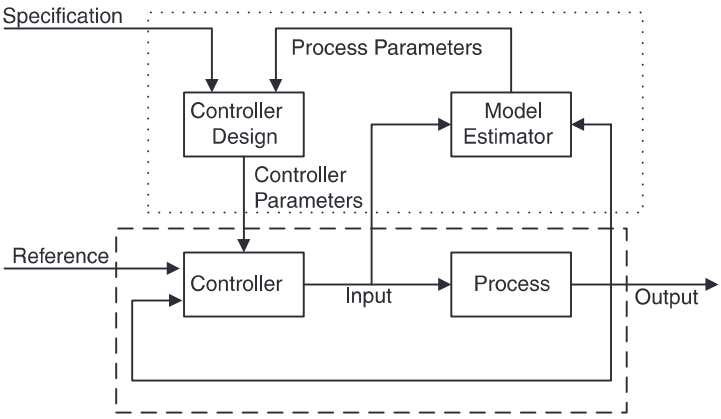

Figure 2.3 Block diagram of an adaptive self-tuning regulator

2.2.1 Model Estimation

Assuming that the process dynamics may be modeled by a discrete time auto-regressive with external input (ARX) model:

$$A(z)y(t) = B(z)u(t-n_d) + e(t) \tag{2.1}$$

where $A(z) = 1 + a_1 z^{-1} + \ldots + a_{n_a} z^{-n_a}$

$$B(z) = (b_0 + b_1 z^{-1} + \ldots + b_{n_b-1} z^{-n_b+1}) \cdot z^{-n_d}$$

and u are the inputs to the process, y are the corresponding observed process outputs, z is the z-transform (time shift) operator, and n_a, n_b, and n_d are the orders of the A and B polynomials and the process delay, respectively.

We introduce the process model parameter vector

$$\theta^T = [a_1 \quad \ldots \quad a_{n_a} \quad b_0 \quad \ldots \quad b_{n_b-1}] \tag{2.2}$$

the regression vector

$$\varphi^T(t) = [-y(t-1) \quad \cdots \quad -y(t-n) \quad u(t-n_d) \quad \ldots \quad u(t-n_d-m+1)] \tag{2.3}$$

and the loss function

$$V(\theta,t) = \frac{1}{2}\sum_{i=1}^{t} (y(i) - \varphi^T(i)\theta)^2 \tag{2.4}$$

The model parameter θ, which minimizes $V(\theta,t)$, the differences between the output observation, $y(i)$, and its prediction, $\varphi^T(i)\theta$, in the least-squares sense, is given recursively by

$$\theta(t) = \theta(t-1) + K(t)(y(t) - \varphi(t)^T \theta(t-1)) \tag{2.5}$$

$$K(t) = P(t-1)\varphi(t)(\lambda I + \varphi(t)^T P(t-1)\varphi(t))^{-1} \tag{2.6}$$

$$P(t) = (I - K(t)\varphi^T(t))P(t-1)/\lambda \tag{2.7}$$

Note that λ in Equations (2.6) and (2.7) is a forgetting factor that dictates how fast the model is updated. The value of λ is $0 < \lambda \leq 1$; the smaller λ is, the faster the estimator can track the model changing. A small λ will also make the estimation more sensitive to measurement noise. In this project, λ is set to be 0.98 for injection velocity control and 0.99 for packing pressure control as the selections produce good estimates. As a rule of thumb, the estimate is based on the last N-step results, and N can be calculated as below [4]:

$$N = \frac{2}{1-\lambda} \tag{2.8}$$

2.2.2 Model Predictive Control (MPC): Generalized Model Control (GPC)

2.2.2.1 Basic Principle of MPC and GPC

Model predictive control (MPC) [5] is a class of advanced process control algorithms. It was originally developed for process industries such as chemical and petrochemical plants in the late 1970s. The research on MPC, both academically and in industrial applications, grew rapidly during the last several decades. The wide application of MPC is mainly due to the following:

1. MPC can be used to deal with complicated process dynamics, including nonlinearity and time-varying characteristics, long time delay, and open-loop instability.
2. MPC can deal with constraints in the process control naturally and systematically.
3. MPC can be extended to multivariable control easily.
4. Feed-forward control is inherently built in to the MPC design, so the process disturbances can be compensated for.
5. MPC is suitable for batch processes since the reference trajectories of the process settings are known before the cycle starts.

6. MPC is a totally open control methodology following certain basic principles for further development and extension.

Due to the above advantages, various MPC algorithms have been proposed: model algorithmic control (MAC), dynamic matrix control (DMC), generalized model predictive control (GPC), and predictive functional control (PFC). These designs all share the same basic features of MPC:

1. Prediction of future outputs based on an internal dynamic model of the process
2. Calculation of an optimal control sequence by minimizing a predefined objective function
3. A receding horizon strategy that moves the control forward toward future sampling times

The basic principle of model predictive control is schematically shown in Figure 2.4, where the prediction, optimization, and receding of the MPC are clearly illustrated.

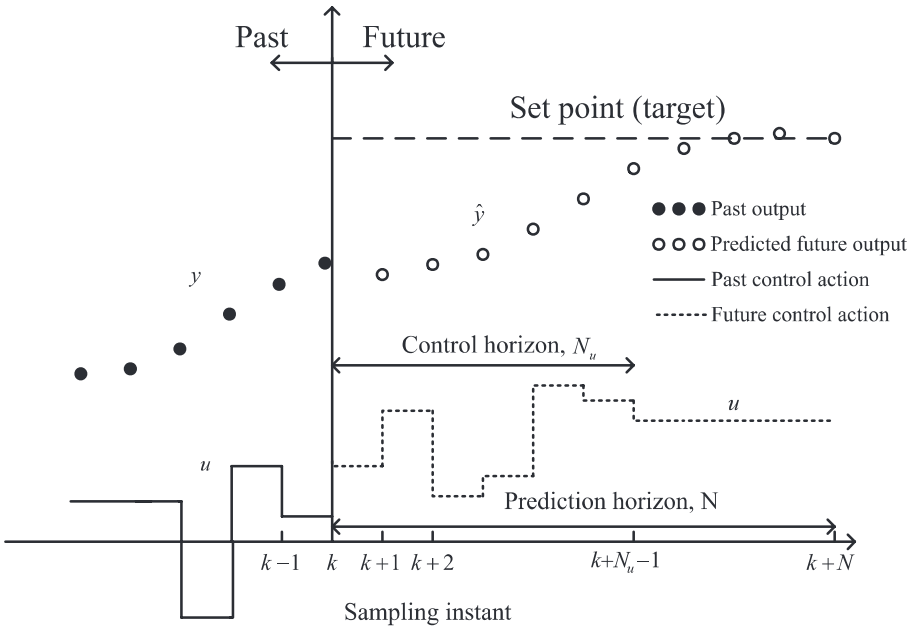

Figure 2.4 Schematics of the model predictive control algorithm

In this chapter, the GPC design is applied to demonstrate the good performance of MPC. The GPC design was first proposed by Clark, Mohtadi, and Tuffs [6]. This control has been shown to be effective with model uncertainty in many process industry applications. To overcome the nonlinear time-varying characteristics of the injection molding process, an adaptive GPC scheme as shown in Figure 2.3 is

2.4.5 P-Type ILC for Packing Pressure

To further demonstrate the performance of iterative learning type control algorithms, the P-type ILC is extended to packing pressure control. Due to the severe time-varying characteristics of the packing pressure dynamics and relatively larger time constant, the sampling rate of the controller is determined to be 50 ms, much longer than that of the injection velocity. The proportional learning rate is selected to be 0.001, also with a series of trial-and-error tests. The designed ILC is applied to experimentally control the packing pressure, and the results are shown in Figure 2.25.

The first cycle's control valve opening is set to be open-loop again, and the pressure response is far from the set-point profile. After five cycles of learning, the sixth cycle's pressure is close to the set point, especially for the first half of the packing. The SSE converging procedure is shown in Figure 2.26. The successful application of packing pressure control again proved the good potential of iterative learning type control algorithms.

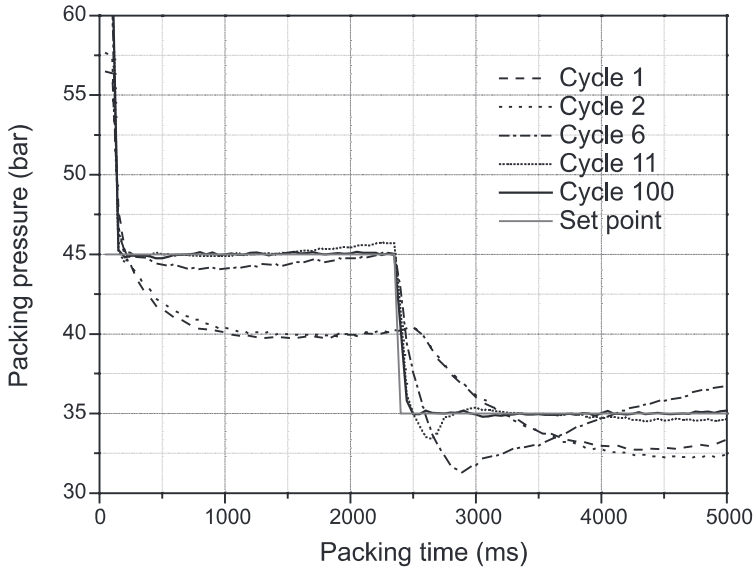

Figure 2.25 Packing pressure P-type ILC result

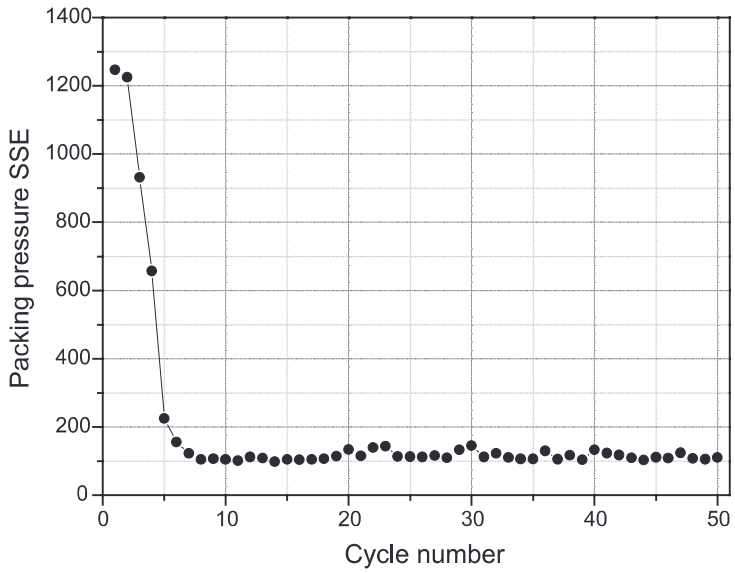

Figure 2.26 SSE converging procedure of the P-type ILC for packing pressure

2.5 Two-Dimensional Control Algorithm

2.5.1 Two-Dimensional Control Background

Injection molding is a typical batch process; it has its own characteristics in comparison to a continuous process. The obvious differences between a continuous process and a batch process like injection molding are (1) a batch process has a finite duration, (2) a batch process repeats itself until the specified amount of products has been made, and (3) a batch process is processed by an ordered set of activities. These characteristics make the control schemes proposed for a continuous process ill-suited for injection molding. Modifications of the original control algorithms have to be made to cope with these features. To summarize the difference between injection molding and traditional continuous processes, the distinctive nature of an injection molding process has three aspects:

- Repetitive nature: the injection molding process repeats itself batch to batch to produce the same products.
- Two-dimensional (in time) dynamics nature: there are within-batch and batch-to-batch dynamics in injection molding simultaneously.
- Multiphase nature: an injection molding process consists of more than one phase.

We found that a water level of ~0.4 wt % decreased the warpage by approximately 0.6 to 0.2 mm and 0.4 to 0.1 mm at cycle times of 31 and 41 seconds for TPO containing 0.5 wt % AC and NC, respectively. Even a water level of 0.24 to 0.26 wt % could decrease the warpage by approximately 0.5 to 0.1 mm and 0.3 to 0.1 mm at the same cycle time for TPO containing 0.5 wt % AC and NC, respectively. The effect of water on warpage reduction was more significant at short cycle times, and AC was more efficient than tubular clay because of its better water-retention capacity. It is clearly seen from both figures that the solid parts could not be demolded at 26 seconds of cycle time without sprue breakage.

5.5.2 Flow Marks and Surface Quality

Similar to microcellular injection molding, flow marks (swirling patterns) were observed on the surface of molded parts in the presence of water. The higher the water content, the more noticeable are the water marks on the surface of the molded part. As discussed in the earlier section, the flow marks are caused by water released as steam at the melt front during filling. Quantitative measurement of the flow marks was done by measuring the surface roughness of the sample. Measurement was done using Veeco Wyco NT9100 laser profilometer. The measurements, using both flat plate and disk specimens of ASTM molded parts, are summarized below.

Flat Plate Mold

Figures 5.19 and 5.20 show the surface roughness of the samples discussed in the previous section, which were molded at different cycle times and at two water levels. The surface roughness of solid TPO with 0.5 wt % NC, which was molded at 41 seconds of cycle time, is included for reference (the last column in the plot). We found that the surface roughness more than doubled as the water content was increased from 0.24 to 0.35 wt %. However, the surface roughness was nearly independent of the cycle time, implying that flow marks were formed mainly during the filling stage.

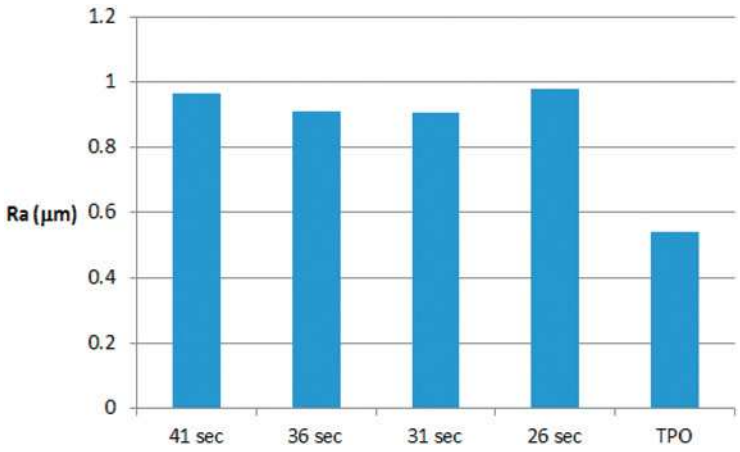

Figure 5.19 Surface roughness of TPO with 0.5 wt % NC and 0.24 wt % water

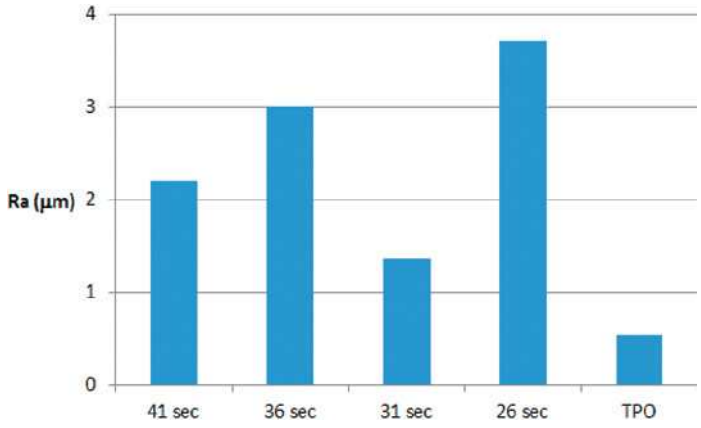

Figure 5.20 Surface roughness of TPO with 0.5 wt % NC and 0.35 wt % water

ASTM Mold

The flow marks on parts molded using the ASTM mold were quantified by measuring the surface quality of the impact disk specimen. In the molding experiment, the melting temperature of the polymer (205 °C and 250 °C) and the injection speed (from 1 to 0.1 second) were varied to investigate their effects on surface roughness (Ra). The initial water content for pressurized TPO with 0.5 wt % AC was 0.42%. The surface roughness of solid TPO parts is also included as a base comparison and summarized in Table 5.8.

Table 5.8 Summary of Surface Roughness Measurements of TPO Molded at Various Conditions

Material and Molding Conditions	Injection Time (s)	TPO 0.5 wt % AC Ra (μm)
Solid, T_{melt} = 205 °C	1	0.51
Press, T_{melt} = 205 °C	1	3.61
	0.25	1.41
Press, T_{melt} = 250 °C	1	1.54
	0.25	1.19
	0.1	1.07

The residual water content of molded parts of pressurized TPO with 0.5 wt % AC was measured to be ~0.2 and 0.1 wt % at melting temperatures of 205 °C and 250 °C, respectively. This indicates that a higher melting temperature would decrease the residual water content, and more water was lost during the molding process. We found that it is very likely that, at higher melt temperature, more water was evaporated inside the barrel during the melting stage, and therefore less water was available in the melt during filling, resulting in a lower value of Ra. We found that the injection time affected the surface roughness since a higher injection speed allowed less time for the steam to escape. In this case, the surface roughness measurements showed a lower Ra as the injection speed was increased.

5.5.3 Hiding the Flow Marks Using In-Mold Coating

A molding trial using pressurized water pellets was carried out at CK Technologies Inc. (Montpelier, OH), which specializes in molding parts for the commercial truck and bus markets. The TPO supplied by CK Technologies was similar to the one previously used and was compounded with 0.5 wt % AC and pressurized to obtain an initial water content of 0.4 wt %. The experiment was done using a Battenfeld injection-molding machine with a flat plate mold with dimensions of 15.3 × 10.87 × 0.32 cm. This mold was equipped with an in-mold coating (IMC) injection port, which was located at the top of the sleeve facing the back platen. The IMC material used was a commercial IMC material provided by OMNOVA Solutions. The IMC coating material was initiated with 0.25% Luperox-26 (*tert*-butyl peroxy-2-ethylhexanoate manufactured by Akzo Nobel Polymer Chemicals LLC for low-temperature applications) and 1.75% TBPB (*tert*-butyl peroxybenzoate manufactured by Arkema Canada Inc. for high-temperature applications). The coating was injected while the part was still in the mold, which was 18 seconds after the packing stage. The curing time for the coating was 72 seconds.

We found that lower packing pressures could be used to obtain a completely filled part using the pressurized pellets. For the solid, the minimum packing pressure needed to obtain a part without a short shot was 3.5 times larger than for the pres-

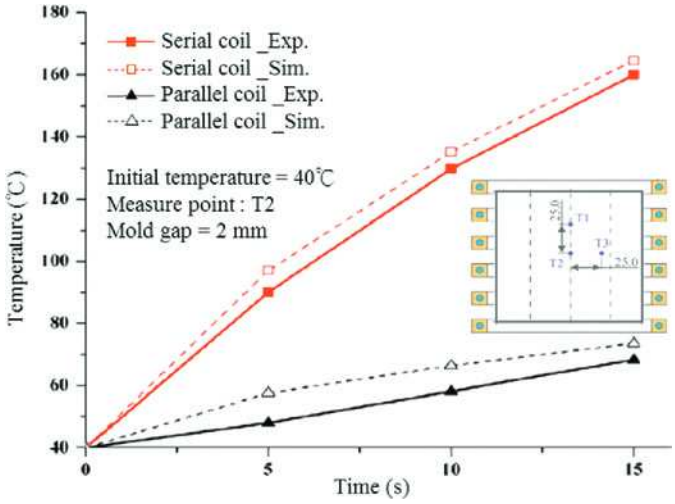

Figure 6.33 Variations of surface temperature at point T2 with regard to time for various coil designs [6]

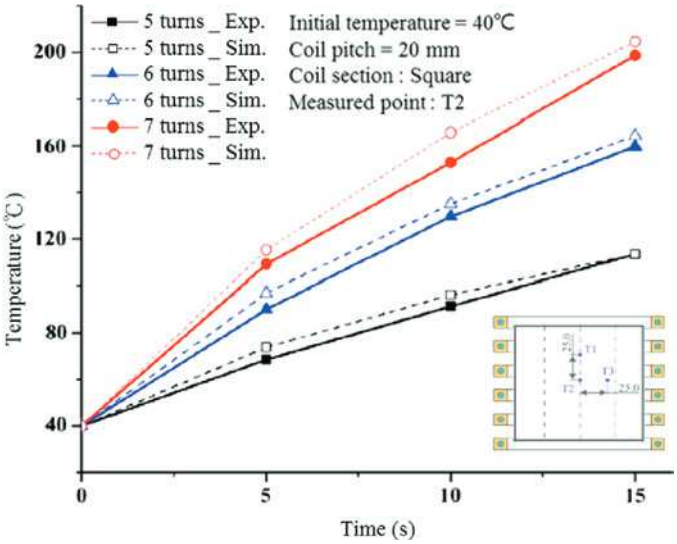

Figure 6.34 Comparison of temperature at point T2 with regard to time given a different number of turns [6]

6.4.7 Induction Heating from the Mold Interior Using Embedded Coils

In the internal coil induction heating (ICIH) method, water cooling is integrated into the injection mold base; hence, the overall heating and cooling effects should be considered together. Figure 6.35 shows schematically the configuration of the

ICIH. When the induction coil is embedded inside the mold, the heat will transfer from the bottom portion of the mold plate to the top surface after heating. One feasible practical configuration is depicted in Figure 6.36.

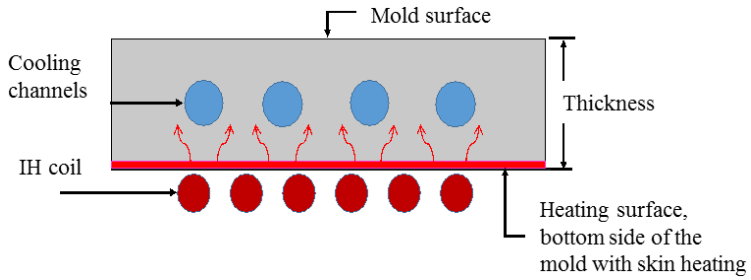

Figure 6.35 Configuration of internal induction heating; the induced heat energy will transfer from the heating surface on the bottom side to the upper cavity surface

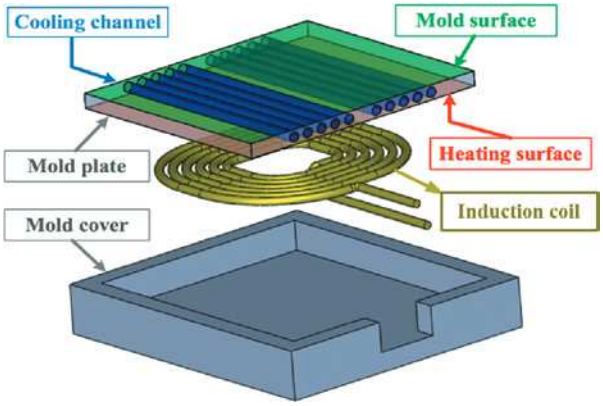

Figure 6.36 Mold structure with embedded internal coil and cooling channels [9]

For internal induction heating, the distance from the induction coil to the cavity surface is one of the most important design parameters. For a top mold plate of 15 mm and 20 mm in thickness, the heating speed was evaluated [32–35] and can be seen in Figure 6.37 under specific operating conditions.

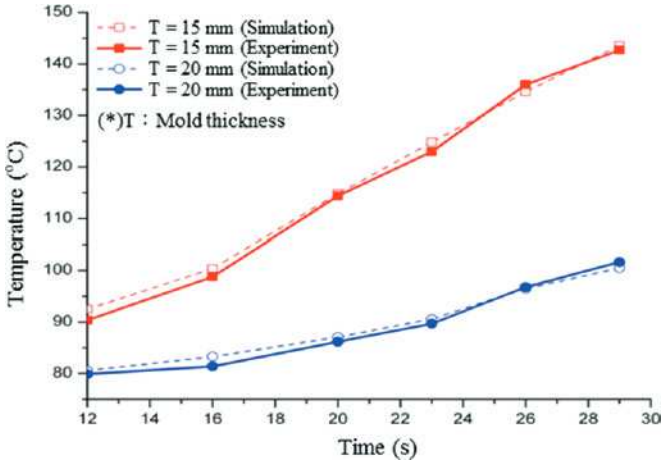

Figure 6.37 Comparison of heating speed results with a mold thicknesses of 15 mm and 20 mm [9]

In the general design of ICIH, if the cooling channels are laid out between the coils and mold surface, control associated with water cooling has a strong influence on the temperature distribution. When the water flows continuously during the heating period, it will lower the heating efficiency and temperature distribution. In contrast, when the water stops running or is drained from the channel, the resulting mold surface temperature will be higher and the temperature distribution will improve as well, as indicated in Figure 6.38.

Cooling Water Control System	Water Running	Water Stagnant	Water Drained out
Thickness of Mold Plate (15mm)	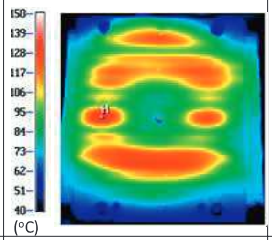	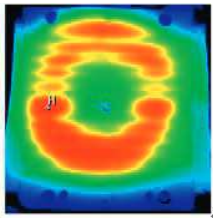	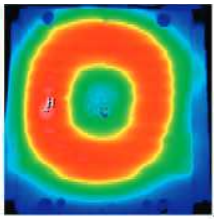
Heating rate (°C/s)	1.3	1.5	1.8

Figure 6.38 Mold plate surface temperature distribution with different methods of water switchover control [32]

For real-world applications of ICIH in the injection molding process, an embedded induction coil is used as the heating source to increase the mold surface temperature. In general, injection molding has three main stages. The mold is first heated

distribution were found for LDPE, although LDPE had a lower melt strength and showed a larger error bar for the cell size experimental data. Simulation results of microcellular injection molding for SCF nitrogen dissolved in PP showed fairly good agreement with experimental data.

7.5 Gas-Assisted Injection Molding

7.5.1 Introduction

The gas-assisted injection molding (GAIM) process utilizes compressed gas as the "packing medium", hence resulting in a lower injection/packing pressure and clamp tonnage compared to those of the conventional injection molding process. Furthermore, GAIM aids in the molding of thick-walled parts, produces significant weight saving, reduces if not eliminates part warpage and sink marks due to reduced filling pressures and residual stresses, and results in shorter cooling times by coring out the thick portion of the part [25].

However, controlling the processing conditions, such as delay time, gas holding time, injected gas pressure, and the amount of injected melt, are critical to ensure consistent gas penetration in the cavity [26]. The most well-known problem is rigidity degradation for rib-strengthened thin plates where the ribs also serve as gas channels in GAIM. When ribs are hollowed by the injected gas during gas-assisted filling, a large void in the core of each gas-channeled rib is created. Thus, rib rigidity is greatly reduced. This problem has been investigated by many researchers [27, 28]. Obviously, the rib design guidelines for conventional molding cannot be applied directly to GAIM.

The 2.5D generalized Hele–Shaw (GHS) approximation has been extensively adopted to model conventional injection molding as well as the GAIM process [29]. However, the nature of the 3D flow inherent in the gas penetration phase invalidates the 2.5D GHS assumptions. Moreover, the irregular cross-section of the gas channel cannot be accurately modeled through the use of a 1D rod element as in the 2.5D approach. An unreliable estimation of geometry-related flow resistance and heat transfer, and furthermore, the prediction errors for the melt front location and gas penetration length, may occur [30, 31].

The gas-assisted injection molding process is a more complicated process than the conventional injection molding process because of its 3D flow characteristics and the instability of the gas bubble. In this section, based on 3D simulation of injection molding, a combination of FVM and a volume-tracking method were further extended to simulate the melt flow as well as the gas penetration in GAIM.

7.5.2 Governing Equations

In this approach, the fluids are considered to be incompressible and Newtonian for the air and injected gas phase or generalized Newtonian fluid for the polymer melt phase. Surface tension at the fluid front is neglected. A set of governing equations to describe the transient and non-isothermal fluid behaviors for channel flow and mold filling have been described in Equations (7.1) to (7.7) in Section 7.2.2. Here, the volume fractional function f is introduced to track the evolution of the melt front and gas penetration. In particular, $f = 0$ is defined as the air or gas phase and $f = 1$ as the polymer melt phase, where the melt front is located within cells with $0 < f < 1$. In this study, the injected gas and the air are assumed to be the same fluids with identical properties. The advancement of f over time is governed by the following transport equation.

$$\frac{\partial f}{\partial t} + \nabla \cdot (\mathbf{u}f) = 0 \tag{7.28}$$

During the polymer melt filling phase, the velocity and temperature are specified at the mold inlet. While the gas is injected, the gas pressure is specified at the gas inlet. On the mold wall, the no-slip boundary condition is applied, and the fixed mold wall temperature is assumed for the energy equation. For the hyperbolic volume fraction advection equation, only the inlet boundary condition is needed, i. e., $f = 1$ for the polymer injection and $f = 0$ for the gas penetration.

The collocated cell-centered FVM-based 3D numerical approach developed in our previous work was further extended to describe the melt flow and gas penetration in GAIM [5]. The numerical method is basically a SIMPLE-like FVM with improved numerical stability. Moreover, second-order accuracy was carefully maintained during discretization. Pressure, velocity, and temperature were solved in a segregated manner. It is this feature that makes the present approach efficient and robust for solving the thermal flow field in complex three-dimensional geometries.

Furthermore, the volume-tracking method based on a fixed framework was incorporated into the flow solver to track the evolution of the melt–gas and melt–air interfaces during injection. After solving the thermal flow governing equations by FVM, the advancement of the interface at each time step was determined by solving the volume fraction advection equation according to the velocities obtained. The material properties from the updated volume fraction function were calculated, and then the next computation of flow field was initiated. This procedure was repeated until the cavity was completely filled.

7.5.3 Case Study

To realize how gas-assisted injection molding works, both numerical simulation and experimental studies were performed. The model was a spiral tube with a radius of 10 mm [32]. The key dimensions are shown in Figure 7.30. The material was polystyrene (PS, manufactured by Chi-Mei). A 78-ton Battenfeld 750/750 co-injection molding machine was used in this study and the gas injection system was provided by Airmold of Battenfeld with an equipped capability of five-stage pressure profile control. The molding conditions are shown in Table 7.3; the remaining conditions included a mold temperature of 60 °C and a gas injection time of 5 s.

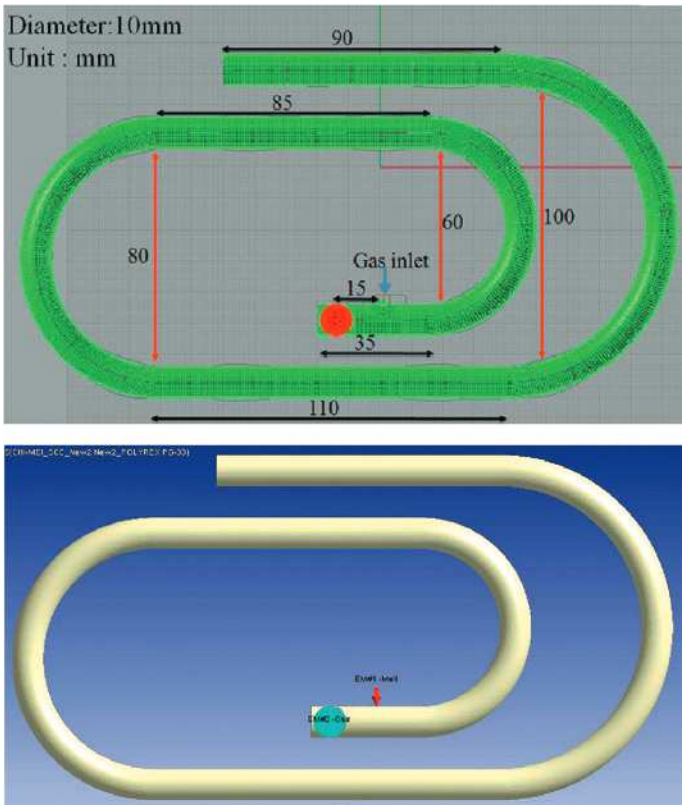

Figure 7.30 Model dimensions and location of gas inlet

In the gas-assisted injection molding process, the melt is hollowed out by gas and forms a skin thickness represented by S as shown in Figure 7.31. The sections of the tube are cut along the gas flow direction and the solidified skin thickness is measured with a caliper. The hollowed-core thickness ratio H equals $(R - S)/R$.

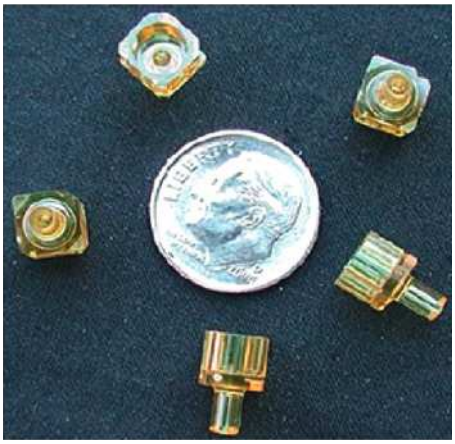

Figure 9.1
Microinjection-molded fiber optics housings [1]

9.2 Issues in Molding Parts with Microfeatures

Injection molding of a part with microfeatures, especially microfeatures with high aspect ratios, requires new technological advances and a thorough understanding of the process. Unlike standard injection molding, rapid polymer cooling is amplified in microinjection molding due to the higher ratio of contact surface between the melt and the cold mold wall to part volume. Rapid polymer cooling in microchannels leads to the formation of a frozen layer that stops the melt flow, as shown in Figure 9.2, resulting in incomplete filling or a short shot. Figure 9.3 shows a comparison of typical gap-wise temperature profiles near the end of the fill as the part thickness decreases. For thick sections, the temperature profile through the thickness displays two peaks due to viscous heating. In the case of thin sections, the two temperature peaks vanish, and the increased heat transfer due to conduction results in a decreased average temperature. Further reductions in thickness result in a duplication of the mold temperature across the part thickness, as is the case for ultrathin sections and microstructures. Consequently, a fast melt solidification hinders the melt flow, resulting in a short shot.

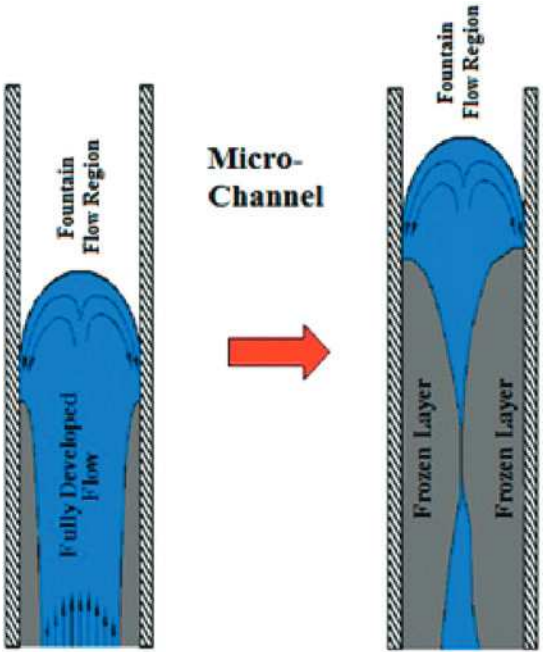

Figure 9.2 Growing frozen layer causes incomplete filling in microchannels

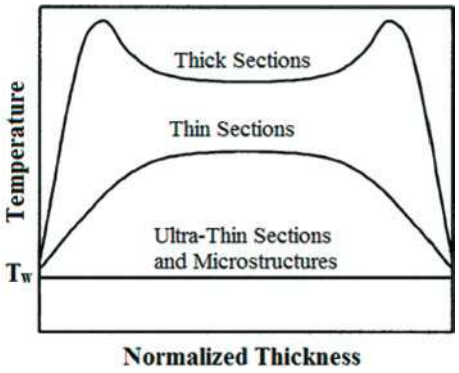

Figure 9.3
Typical gap-wise temperature changes at the end of the fill stage, as part thickness is decreased [2]

In injection molding, the polymer melt freezing time during filling can be predicted from the one-dimensional heat conduction equation:

$$\frac{\partial T}{\partial t} = \frac{k}{\rho C_p}\left(\frac{\partial^2 T}{\partial z^2}\right) \tag{9.1}$$

where ρ is the density, C_p is the specific heat, and k is the thermal conductivity.

Based on Equation (9.1), Equation (9.2) predicts the time for the part center temperature to become equal to the freezing temperature:

$$t_f = \frac{H^2}{\alpha\pi^2} \ln\left(\frac{4(T_p - T_m)}{\pi(T_f - T_m)}\right) \tag{9.2}$$

where t_f is the freezing time, H is the part thickness, α is the thermal diffusivity ($\alpha = k/\rho C_p$), T_p is the initial polymer melt temperature, T_m is the mold temperature, and T_f is the polymer freezing temperature.

Figure 9.4 illustrates a plot of Equation (9.2) for a typical case of $\alpha = 10^{-7}$ m^2/s, $T_p - T_m = 100$ °C, and $T_f - T_m = 30$ °C [3]. The plot shows a linear log–log relationship between part thickness and freezing time. Consequently, as the part thickness decreases, so does the time allowed for the polymer melt to fill the cavity. In the case of ultrathin cavities, the polymer freezes rapidly if a cold mold is used (<0.05 s). Although such an effect can be reduced by using a heated mold, the improvement comes at the expense of an increased cycle time due to the increased cooling time.

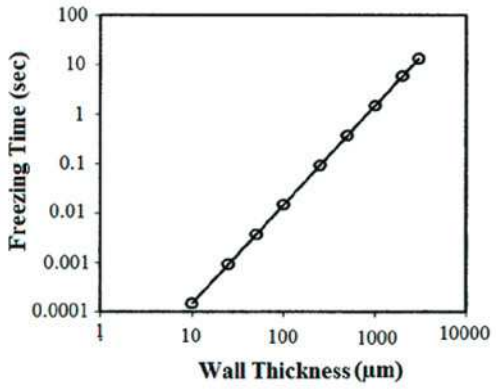

Figure 9.4
Estimated freezing time [3]

In contrast to conventional injection molding, a physical phenomenon called the hesitation effect has to be taken into account when molding microfeatures. To understand the hesitation effect, consider the flow pattern throughout the mold cavity as shown in Figure 9.5. The hesitation effect is common when an injection-molded part contains microfeatures oriented 90° from the main cavity. As shown in the figure, during the injection stage of the melt, filling of the microrib cavity decreases as it moves farther from the gate due to the decrease in injection pressure from the gate to the melt flow front.

The melt that just entered the microrib loses heat until the rest of the mold cavity is filled. When the mold is almost completely filled, the available injection pressure